Electron Beam Induced Luminescence of SiO_2 Optical Coatings

JR Dennison[1], Amberly Evans[1], Gregory Wilson[1], Justin Dekany[1], Charles W. Bowers[2] and Robert Meloy[3]

[1]Materials Physics Group, Utah State University
4415 Old Main Hill, Logan, UT 84322 USA

[2]NASA Goddard Space Flight Center
Code 667, Greenbelt, MD 20771 USA

[3]MEI Technologies, Inc.
NASA Goddard Space Flight Center

Abstract- **Optical coatings of disordered thin film SiO_2/SiO_x dielectric samples on reflective metal substrates exhibited cathodoluminescence under electron beam irradiation. Measurements of the absolute radiance and emission spectra as functions of incident electron energy, flux and power over a range of sample temperatures are reported. Radiance reached a saturation plateau at high incident electron power. Well below saturation radiance scaled with deposited power, that is linearly with incident power for lower-energy non-penetrating electrons and decreasing with increasing energy for penetrating radiation. Four bands were observed in spectral measurements from 300 nm to 1000 nm. Changes in peak intensity and shifts in peak energies as functions of temperature are described. The observations are explained in terms of a simple disordered band theory model and the transitions that take place between electrons in extended conduction states and localized trapped states associated with structural or compositional defects in the highly disordered insulating materials; this provides a fundamental basis for understanding the dependence of cathodoluminescence on irradiation time, incident flux and energy, and sample thickness and temperature.**

I. Introduction

Disordered, thin-films of fused silica undergoing electron beam irradiation have been shown to produce a low-efficiency cathodoluminescence [1,2]. Optical coatings or substrates incorporating SiO_2/SiO_x are common and the induced cathodoluminescence can be beneficial or detrimental depending on the application. Optical sensors for vacuum applications such as electron spectroscopy and microscopy or luminescence spectroscopy, as well as hybrid electro-optical semiconductor devices are just a few of useful applications of this cathodoluminescent property. On the other hand, such luminescence can potentially produce a stray light background in space-based astronomical observatories which are exposed to high energy electron fluxes from space plasmas. Space plasmas typically are dominated by fluxes (~0.1 pA/cm^2 to >10 nA/cm^2) for electron energies of up to ~100 keV [3]. In the case of IR observatories or sensors, the applications often require low temperatures down to 10's of Kelvin.

These applications motivated a study of the dependence of the cathodoluminescent intensity of incident electron flux, energy and power and on material temperature and thickness. Measurements are presented of the absolute radiance and emission spectra as functions of incident electron energy, flux and power for fused silica coatings (~60 nm to ~200 nm thick) on reflective metal substrates over a range of sample temperatures and emission wavelengths. These measurements are explained in terms of electron interactions with the materials and a simple disordered band theory model based on atomic-scale stochastic transport of electrons in highly disordered insulating materials (HDIM).

II. Experimental Methods

Experiments were conducted in an ultrahigh vacuum electron emission test chamber [4], modified for observations of low intensity UV/VIS/NIR emissions over a broad range of sample temperatures [5,6]. Details of the experimental set up; electron sources and beam characterization; optical detectors, methods, and calibration; the sample mounting carousel and thermal stage; and a general schematic of the experimental system used are given in [6]. Additional details of the thermal dependence of the cathodoluminescence are presented in [6]. Electron transport and surface voltage data acquired simultaneously with luminescence data are reported in [7].

Electrons were directed to the samples using well-characterized, low-flux electron beams (~50 pA/cm^2 to 1 μA/cm^2) with an energy range of 5-25 keV. A Faraday cup monitored the defocused normally-incident beam, which had about ±30% uniformity over an ~3 cm dia. beam spot. Two fiber optic spectrometers and four cameras monitored low intensity light emission: UV/VIS (Stellarnet, 13LK-C-SR; ~200-1080 nm) and NIR (Stellarnet, RW-InGaAs-512; ~1000-1700 nm) spectrometers, a VIS/NIR image-intensified CCD video camera (Xybion, ISG-780-U-3; ~400-900 nm), and a visible-range SLR CCD camera. Additional InGaAs (~0.8-1.7 μm) and InSb (~1-5.5 μm) video cameras and filter combinations were used; no appreciable IR radiation (1-2.5 μm) was observed for any of the experiments reported here.

Coated mirror samples (2.5 cm dia.) had optically smooth, thin films (~65 nm thick) disordered SiO_2/SiO_x (fused silica) deposited on thin, but optically opaque, highly reflective, smooth metal (Au or Ag) layers, on thick fused quartz or metallic substrates. The samples were optically cleaned, underwent a ~12 hr vacuum bakeout at ~390 K and $<1\cdot10^{-3}$ Pa to eliminate adsorbed water and volatile contaminates, and were place in a vacuum chamber (base pressure $<1\cdot10^{-6}$ Pa) for >24 hrs. Samples mounted on Cu carousels and thermally anchored to (but electrically isolated from) thermal reservoirs, were maintained over ~40<T<400 K with ±3 K long-term stability.

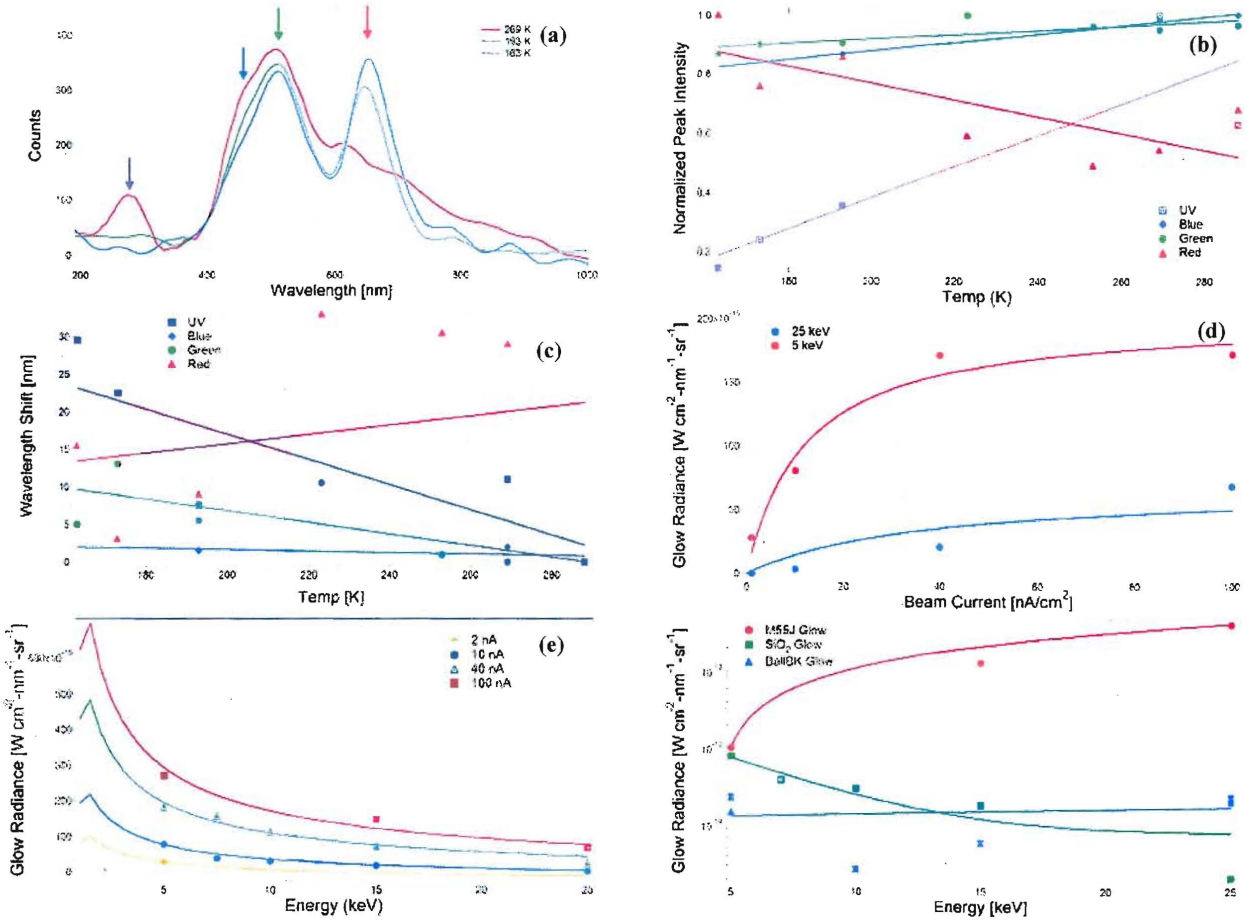

Fig. 1. Optical measurements of luminescent thin film disordered SiO_2 samples. **(a)** Three luminescence UV/VIS spectra at decreasing sample temperature. Four peaks are identified: red (~645 nm), green (~500 nm), blue (~455 nm) and UV (275 nm). **(b)** Peak amplitudes as a function of sample temperature, with baseline subtracted and normalized to maximum amplitudes. **(c)** Peak wavelength shift as a function of sample temperature. **(d)** Total luminescent radiance versus beam current at fixed incident energy fit by (1). **(e)** Total luminescent radiance versus beam energy at fixed incident flux fit by (1). **(f)** Total luminescent radiance versus beam energy at fixed 10 nA/cm^2 incident flux for epoxy-resin M55J carbon composite (red; linear fit), SiO_2 coated mirror (green; fit with (1)), and carbon-loaded polyimide black Kapton 230XC275 (blue; triangles for 10 nA/cm^2 and hour glasses for 30 nA/cm^2 scaled to 10 nA/cm^2, constant fit).

III. Results

The thin film fused silica samples exhibited luminescent intensity, I_y, readily observable with the unaided eye in a darkened room, which scaled with electron beam intensity and responded to changes in beam position and profile on rapid time scales [6]. At high incident electron flux J_b, I_y exhibited saturation as shown in Fig. 1(d) for data ranging from 2-100 nA/cm^2 at constant 5 keV and 25 keV incident energies and ~40 K. For the full range of incident fluxes at ~40 K, the emission intensity decreased with increasing incident energy from 5 keV to 25 keV, with a saturation dose rate $\dot{D}_{sat} \approx 1.5 \cdot 10^5$ rad/s (Fig. 1(e)). At both higher incident fluxes and energies, the fused silica emission intensity scaled at rates less than linear with *incident* power; rather emission intensity scaled with *absorbed* power per unit mass (dose rate) as is found for radiation induced conductivity. Similar behavior for the overall luminescent intensity was observed at ~40 K<T<340 K and the full range of energies.

Overall intensity of the glow in the visible range for a given incident energy and flux increased roughly inversely with T as it decreased from ~300 K to ~40 K. A clear variation in the color as a function of temperature was also observed; as temperature decreased, the images of the samples became redder and less blue. This was confirmed by the dependence of the luminescence emission spectra as a function of T, as shown in Figs. 1(b) and 1(c). Three peaks were observed, centered at ~275 nm, ~500 nm and ~645 nm, and an additional shoulder at ~455 nm. These peaks were consistent with the results for similar disordered SiO_2 studies at room temperature [1,2]. The peaks at 645 nm and at 275 nm and 500 nm are attributed to a nonbridging oxygen hole center [1] and an oxygen deficient center [2], respectively. The variation in spectral intensity with temperature is shown for three representative temperatures in Fig. 1(a). There is an observed decrease in intensity of the red peak (near 645 nm) and increase of the other peaks with increasing temperature, as illustrated in Figs. 1(a) and 1(b). A shift of luminescent peaks to shorter wavelengths with increasing temperature was observed for all but the red peak (Fig. 1(c)).

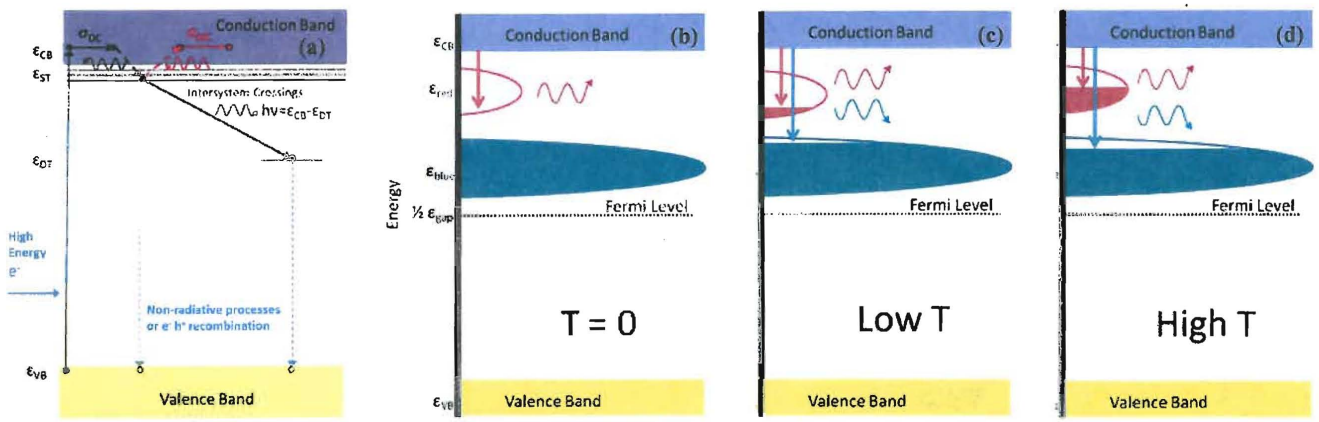

Fig. 2. Qualitative two-band model of occupied densities of state (DOS) as a function of temperature during cathodoluminescence. **(a)** Modified Joblonski diagram for electron-induced phosphorescence. Shown are the extended state valence (VB) and conduction (CB) bands, shallow trap (ST) states at ε_{ST} within $\sim k_B T$ below the CB edge, and two deep trap (DT) distributions centered at $\varepsilon_{DT}=\varepsilon_{red}$ and $\varepsilon_{DT}=\varepsilon_{blue}$. Energy depths are exaggerated for clarity. **(b)** At $T\approx 0$ K, the deeper DT band is filled, so that there is no blue photon emission if $\varepsilon_{blue}<\varepsilon_{eff}$. **(c)** At low T, electrons in deeper DT band are thermally excited to create a partially filled upper DT band (decreasing the available DOS for red photon emission) and a partially empty lower DT band (increasing the available DOS for blue photon emission) **(d)** At higher T, enhanced thermal excitations further decrease red photon emission and increase blue photon emission. Radiation induced conductivity (RIC; red in Fig. 2(a)) is also enhanced at higher T, as electrons in ST are thermally excited into the CB.

IV. Model of Cathodluminescent Intensity

The basic model for the observed electron-induced luminescence phenomenon is based on band theory of HDIM, as depicted in Fig. 2. I_γ is proportional to the number of available states and the rates of each transition depicted in the modified Joblonski diagram [8,9] of Fig. 2(a). We find I_γ scales with incident current density J_b, beam energy E_b, temperature T, and photon wavelength λ as

$$I_\gamma(J_b, E_b, T, \lambda) \propto \dot{D}(J_b, E_b)\left[\frac{1}{\dot{D}+\dot{D}_{sat}}\left(\frac{\varepsilon_{ST}}{k_B T}\right)\right]\{\mathbb{A}_f(\lambda)[1+\mathbb{R}_m(\lambda)]\} \quad (1)$$

where dose rate $\dot{D}$ (absorbed power per unit mass) is given by

$$\dot{D}(J_b, E_b) = \frac{E_b J_b[1-\eta(E_b)]}{q_e \rho_m} \times \begin{cases} [1/L] & ; R(E_b) < L \\ [1/R(E_b)] & ; R(E_b) > L \end{cases} \quad (2)$$

I_γ is proportional to the number of electrons excited into the conduction band (CB) that can then transition rapidly through internal conversions to shallow trap (ST) states just below the CB due to defects in the crystalline structure or chemical defects from substitutional dopants. For the HDIM SiO_2 (band gap, $\varepsilon_{gap}\approx 8.9$ eV), excitation from the valence band (VB) to CB is not thermal, but rather occurs through collisions of the incident high energy electrons. Thus I_γ is proportional to $\dot{D}$, given by (2) as the number areal density of incident electrons (J_b/q_e) times energy per incident electron E_b divided by the mass for energy deposition $(\rho_m L \cdot Area)$. For nonpenetrating radiation—where the energy-dependent penetration depth or range $R(E_b)$ is less than the film thickness L—all incident power is absorbed in the coating and I_γ and $\dot{D}$ are linearly proportional to the incident power density, $(J_b E_b/q_e)$. For penetrating radiation—where $R(E_b) > L$—the absorbed power is reduced by a factor of $[L/R(E_b)]$ [6,7]. Fig. 3 shows $R(E_b)$ for disordered SiO_2, along with a corresponding $\dot{D}(E_b)$ curve based on (2) [7]. At energies up to ~1.5 keV needed to penetrate a ~65 nm SiO_2 coating, I_γ is linearly proportional to incident flux, energy and power; we have seen this linear dependence for thicker epoxy resin coatings of carbon composites (see Fig. 1(f)) [10] and for thicker similar silica coatings at lower 0.2-5 keV energies. However, above the coating penetration energy the energy-dependence of R and $\dot{D}$ cause I_γ to decrease with incident energy (see Fig. 1(b)).

An energy-dependent correction to the incident flux, $J_b[1-\eta(E_b)]$, is included in (2) to account for quasi-elastic backscattered electrons that do not deposit substantial energy; for Au, where most backscatter occurs for $2<E_b<25$ keV, the backscatter yield $\eta\approx 0.2$ is largely independent of E_b [11]. For biased samples, or when excess charge is stored in the trap states, a surface voltage V_s results and E_b is replaced everywhere in (2) by the landing energy, $(E_b - q_e V_s)$. This additional trapped charge also increases the level of occupancy in the disordered bands; the Fermi level, ε_F, is replaced by an effective Fermi level, ε_{eff} which is in essence a charge- (and temperature-) dependent chemical potential.

I_γ is also proportional to the ST density of states (DOS) available and to their trapping and retention rates. At very high current density, saturation can occur when ST or deep trap (DT) bands fill, limiting the number of state electrons can decay into. Similar suppression of I_γ can result from a modified Stern-Volmer process for quenching due to non-radiative excited state reactions of the ST, where the ratio of quenched to unquenched emission is equal the ratio of unquenched-to-quenched lifetimes, $I_Q/I_o = \tau_o/\tau_Q = 1 + k_Q \tau_o n_Q$ [9]. One such reaction occurs when electrons in ST are thermally excited to the CB, leading to radiation induced conductivity (RIC) in the presence of an electric field. RIC is complimentary to luminosity, with $\tau_Q \equiv k_Q n_Q \propto \sigma_{RIC} = k_{RIC}(T)\dot{D}^{\Delta(T)}$. When RIC is the only quenching reaction, a simple temperature-dependent model for the k_{RIC} and Δ parameters for dielectric materials [12] leads to $I_\gamma \propto [1 - e^{-(E_Q/k_B T)}] \approx (E_Q/k_B T)$ with $E_Q > k_B T$ equal to the mean energy separation of the ST from the CB.

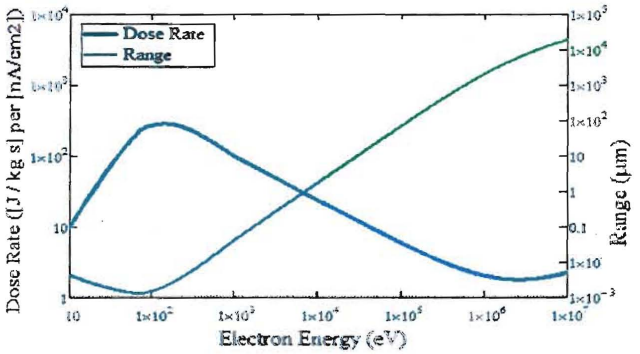

Fig. 3.Range and dose rate of disordered SiO_2 as a function of incident energy using calculation methods and the continuous slow-down approximation described in [5].

A model with multiple DT bands is necessary to qualitatively explain the observed phosphorescence emission spectra. The presence of four identifiable UV/VIS peaks in the spectra suggests that there are at least four bands of optically-active localized defect DT bands well within the band gap, with peak energies below the CB edge at $\gtrsim hc/\lambda$ of the emitted photons. The T-dependent peak intensities are determined by the extent and occupancy of these DT bands, which will be proportional to the number of available, optically-active DT states and a transition probability. The occupancy of a given state is determined to first order by the effective Fermi level for a given density of trapped charges. A more detailed model will take into account the transition probabilities from one DT state to another and non-radiative recombination of electrons with largely immobile VB holes or disordered acceptor states above VB.

Fig. 2 illustrates a two band model for DT distributions centered at ε_{red} and ε_{blue} below the CB edge. Thermal energy controls the thermal excitation of the electrons and the relative filling of the bands. At low T, $\varepsilon_{red}<\varepsilon_{eff}<\varepsilon_{blue}$, so that red transitions are enhanced and others are suppressed. At higher T, red intensity decreases as the band fills at the expense of deeper bands; this also explains the observed peak wavelength dependence with temperature (see Fig. 2(c)).

Finally, the term in curly brackets in (1) accounts for photons propagation through the coating. $\mathbb{A}_f(\lambda)$ is the optical absorption of the coating. For high $\mathbb{A}_f$ materials (*e.g.*, C loaded polyimide in Fig. 1(f)), I_γ is limited by the region from which photons can escape and is approximately independent of electron energy. The 1 in (1) accounts for photons emitted toward the surface and $\mathbb{R}_m(\lambda)$ is the λ-dependent reflectivity of the metallic layer. For highly reflective materials like Ag, $\mathbb{R}_m \approx 1$ at all λ. For materials like Au, the glow spectrum is enhanced at short λ, due to greater reflectivity at shorter λ. For less reflective materials like C, $\mathbb{R}_m \ll 1$ at all λ.

V. Conclusion

Low intensity cathodeluminescence was observed for thin disordered SiO_2 coatings under low intensity incident electron irradiation. The number and wavelengths of peaks were consistent with previous room temperature observations. The luminescence intensity was proportional to dose rate and displayed quenching. A model based on multilevel disordered DOS qualitatively explained the intensity and wavelength versus temperature trends observed from ~160 K to ~280 K.

Continued research will further investigate luminescence vs incident electron energy and flux, electron range, and film thickness and will extended T measurements to develop a quantitative model for intensity and wavelength vs T behavior for observed DT bands. In principle these measurements can be used to map the DOS of the different bands. Investigations of intensity vs electron beam exposure time and decay time after turning the electron beam off will study initial time-dependence as traps fill to the effective Fermi level and empty after excitation into the CB by irradiation has ceased, as well as ties between luminosity and RIC.

Acknowledgment

We acknowledge instrumentation and experimentation contributions from Robert Johnson and Doug Ball, help with optical calibrations from James Peterson and the USU Space Dynamics Laboratory, Michael Taylor for the use of video cameras, and aid with theoretical models from Alec Sim.

References

[1] R. Salh, A. von Czarnowski, M.V. Zamoryanskaya, E.V. Kolesnikova and H.-J. Fitting, "Cathodoluminescence of SiO_x Under-stoichiometric Silica Layers," *Phys. Stat. Sol.*, vol. 203, pp. 2049-2057, Apr. 2006.

[2] A.N. Trukhin, M. Goldberg, J. Jansons, H.-J. Fitting and I.A. Tale, "Silicon Dioxide Thin Film Luminescence in Comparison with Bulk Silica," *J. Non-Crystalline Sol.*, vol. 223, pp. 114-122, Jan. 1998.

[3] D. Hastings and H. Garrett, *Spacecraft-Environment Interactions*, New York, NY: Cambridge Press, 1996.

[4] W.Y. Chang, J.R. Dennison, N. Nickles and R.E. Davies, "Utah State University Ground-based Test Facility for Study of Electronic Properties of Spacecraft Materials," *Proc. 6th Spacecraft Charging Techn. Conf.*, (Hanscom AFB, MA, 2000).

[5] J. Dekany, R.H. Johnson, G. Wilson, A. Evans and JR Dennison, "Ultrahigh Vacuum Cryostat System for Extended Low Temperature Space Environment Testing," *Proc. 12th Spacecraft Charging Techn. Conf.*, (Kitakyushu, Japan, 2012).

[6] A. Evans, G. Wilson, J. Dekany, A.M. Sim and JR Dennison "Low Temperature Cathodoluminescence of Space Observatory Materials," *Proc. 12th Spacecraft Charging Techn. Conf.*, (Kitakyushu, Japan, 2012).

[7] G. Wilson, JR Dennison, A. Evans and J. Dekany "Electron Energy Dependent Charging Effects of Multilayered Dielectric Materials" *Proc. 12th Spacecraft Charging Techn. Conf.*, (Kitakyushu, Japan, 2012).

[8] A. Joblonski, Über den Mechanismmus des Photoluminescence voFarbstoff-phosphoren," *Z. Phys.*, Vol. 94, pp.38-46, 1935.

[9] J.R. Lakowicz, *Principles of Fluorescence Spectroscopy*, Plenum Press, New York, 1983.

[10] V. Griseri, L.A. Dissado, J.C. Fothergill, C. Laurent and G. Teyssedre, "Photoluminescence, recombination induced luminescence and electroluminescence in epoxy resin," *J. Phys. D: Appl. Phys*, vol. 34, pp. 2534-2540, 2001.

[11] R.C. Hoffmann and JR Dennison, "Methods to Determine Total Electron-Induced Electron Yields Over Broad Range of Conductive and Nonconductive Materials," *IEEE Trans. Plasma Sci.*, vol. **40**(2), pp. 298-304 2012

[12] JR Dennison, J. Gillespie, J.L. Hodges, R.C. Hoffmann, J. Abbott, A.W. Hunt and R. Spalding, "Radiation Induced Conductivity of Highly-Insulating Spacecraft Materials," in Appl. of Accelerators in Res. and Industry, *Am. Inst. Phys. Conf. Proc. Ser.*, vol. 1099, ed. F.D. McDaniel and B.L. Doyle, (Am. Inst. Phys., Melville, NY, 2009), pp. 203-208.